BULLETIN OF THE POLISH ACADEMY OF SCIENCES
TECHNICAL SCIENCES, Vol. 72(5), 2024, Article number: e150809
DOI: 10.24425/bpasts.2024.150809

Novel temperature-effective modeling and state of charge estimation based on sigma-point Kalman filter for lithium titanate oxide battery

Yusuf MURATOĞLU[1]* **and Alkan ALKAYA**[2]

[1] Department of Electronics and Automation, Vocational High School, Toros University, Mezitli 33340, Mersin, Turkey
[2] Department of Electrical and Electronics Engineering, Faculty of Engineering, Mersin University, Ciftlikkoy 33100, Mersin, Turkey

Abstract. Battery modeling and state of charge (SoC) estimation are critical functions in the effective battery management system (BMS) operation. Temperature directly affects the performance and changes the model accuracy of a battery. Most studies have focused on estimating the internal temperature of the battery from the surface temperature of the battery with the help of sensors. However, due to the high number of cells in battery packs, the increase in sensor costs and the number of parameters have been ignored. Therefore, this article presents a new framework for the temperature effect using the electrical circuit model. The terminal voltage of the battery includes the effect under different operating conditions. This effect was associated with internal resistance in the battery model. The developed temperature-effective battery model was tested at different temperatures and operating currents. The model was validated with a maximum average root mean square error of 0.05% from the test results. The SoC of the LTO battery was estimated with the sigma-point Kalman (SPK) filter incorporating the developed model. The maximum average root mean square error in the estimation results is 0.11%. It is suitable for practical applications due to its low cost, simplicity, and reliability.

Keywords: temperature-effective modeling; state of charge estimation; sigma-point Kalman filter; battery management system; energy storage system.

1. INTRODUCTION

The mobility of goods and people is key to the economy and society. Since sustainable and clean energy is essential in this mobility, it is necessary to store energy adequately, and quickly and use it efficiently. Energy storage systems (ESS) typically occur through chemical, mechanical, or thermal means [1].

Chemical energy storage (battery) is an important technology in transitioning to a sustainable and clean energy system. Li-ion batteries have long cycle life, high specific energy, and low self-discharge rates. These features enable them to surpass other battery technologies. Li-ion batteries are used in many applications, from electronic devices to the transportation sector [2].

Electric vehicles (EVs) are an alternative solution for the transportation sector, which is largely dependent on fossil fuels. The range and capabilities of EVs depend on the battery technology used, and their safety depends on the battery management system (BMS). The general problems of EVs in terms of capability and performance are fast charging and range problems. Although currently used lithium-ion battery types are solutions to these problems, they are insufficient on their own [3–5]. Lithium titanate oxide (LTO) batteries have higher specific power energy, higher life cycle, and better safety than other types of lithium-ion batteries. These features enable them to provide solutions to range and fast charging problems on their own [6]. BMS is an important unit where data of battery groups is monitored, evaluated, and managed. Current, voltage, and temperature data are collected from battery groups. Using this data, important functions such as battery state of charge (SoC) and state of health (SoH) are obtained. BMS performs cell balancing of battery groups within the safe operating range with all the information [7].

The SoC is obtained from measurable temperature, voltage, and current data of the battery cell. The SoC requires an electro-thermal battery model of the battery for its accuracy under variable load and ambient temperature. The electro-thermal model of the battery should include two submodels. The first is the electrical model, which describes the adaptive electrical behavior of the battery to varying load situations. The second is the thermal model that can express the thermodynamic properties of the battery suitable for variable ambient temperature [8].

Models describing electrical behavior are divided into four basic groups in the literature: empirical model, data-driven model, equivalent circuit model (ECM), and electrochemical model [9]. In empirical models, the nonlinear behavior of the battery is expressed as a mathematical function or reduced-order polynomial. In this method, which is quite simple to apply, the non-linear characteristic of the battery reduces the model accuracy considerably [10]. The electrochemical model directly expresses the internal reactions of the battery. This model, created with partial differential equations, expresses the nonlinear characteristics of the battery better than the empirical model.

*e-mail: yusuf.muratoglu@toros.edu.tr

Manuscript submitted 2024-12-26, revised 2024-04-22, initially accepted for publication 2024-06-08, published in September 2024.

However, it is insufficient due to the complexity of the calculation process in the model and its accuracy under different operating conditions [11]. The data-driven model can directly give the terminal voltage of the battery without depending on its variable relationships. However, this requires a suitable historical measurement dataset. For this reason, it is not widely used [12]. The ECM consists of open circuit voltage (OCV), internal resistance, and resistor-capacitance networks. OCV defines the nonlinear characteristic of the battery, internal resistance defines the voltage drop under load, and resistance-capacity networks define the electrochemical processes. The ECM provides numerous combinations of circuit components and connections. Thevenin model, Rint model, and Partnership for a New Generation of Vehicles (PNGV) model are the most widely used circuit models [13].

There are four main methods in the literature for models describing thermodynamic behavior: direct measurement, electrochemical impedance spectroscopy (EIS), electrochemical-thermal coupling model, and electro-thermal coupling model [14–17]. The direct measurement method is provided by measurements made on the structure of battery cells with the help of thermal sensors. However, it is not a preferred method because it damages the battery structure, and the sensor costs are high. In the EIS and the electrochemical-thermal coupling model method, the results are quite accurate. However, the methods are not practical because they have a complex measurement system and are not economical. The electro-thermal coupling model combines the electrical circuit model and the two-state thermal model (TSTM). In the two-state thermal model, the heat production rate of the battery cell is calculated by the Bernardi heat generation model. Ambient temperature and battery cell surface temperature data are measured. The internal temperature of the battery cell is estimated with the help of the following data: ambient temperature, heat production rate of the battery cell, and surface temperature of the battery cell. The high accuracy of this popularly applied method has been proven by many studies in the literature [18–25]. Unfortunately, this model requires measuring the surface temperature information of each cell. Additionally, the number of model parameters increases considerably. As a result, this method has high sensor costs and a complex management system.

In this study, a temperature-effective model for the LTO battery is designed with a new modification to be applied to the electrical circuit. In the proposed temperature-effective battery model, there is no need for a thermal model and high-cost sensors. It can work adaptively to different operating currents and different ambient temperatures. The SoC of the LTO battery was estimated with the help of the proposed temperature-effective battery model and the sigma-point Kalman filter (SPKF), which is one of the non-linear estimators.

2. METHOD

2.1. Development of temperature-effective battery model

The temperature-effective model in LTO batteries is illustrated in Fig. 1. This model includes the Coulomb counting method, OCV method, internal resistance determination, and Thevenin electrical circuit.

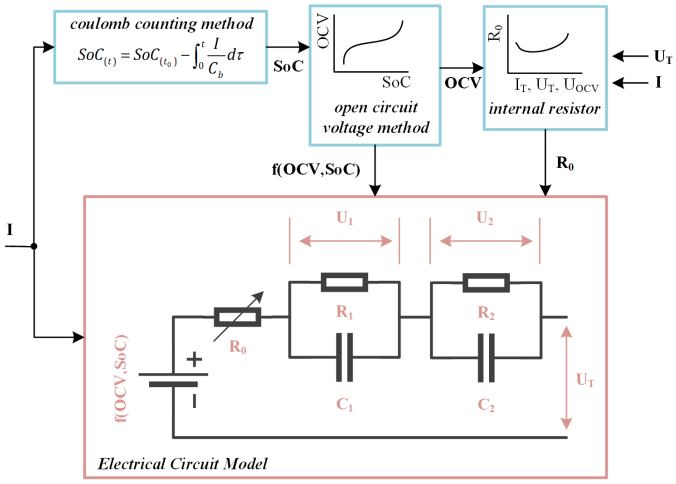

Fig. 1. Temperature-effective model of LTO battery

The Coulomb counting method calculates the relative SoC change based on the integration of the current over time. This change is calculated as shown in equation (1):

$$SoC_{(t)} = SoC_{(t-1)} - \int_0^t \frac{I}{C_b} \mathrm{d}\tau, \tag{1}$$

where $SoC_{(t)}$ is the SoC at time t, $SoC_{(t-1)}$ is the SoC at time $(t-1)$, and C_b is the capacity value of the battery cell.

$f(OCV, SoC)$ is obtained by determining the voltages at the points where the battery is not under load and rested for a sufficient time at the relevant SoC value. The data fitting method based on polynomial interpolation was used for the mathematical model of the obtained data.

The ohmic internal resistance of the battery is an important factor affecting the discharge efficiency and power performance. Internal resistance is affected by various usage conditions such as depth of discharge and temperature. Therefore, it must be adaptive to different usage conditions. The terminal voltage of the battery is directly affected by different usage conditions. In this study, internal resistance is calculated using the battery OCV and voltage under load, as shown in equation (2):

$$R_0 = \frac{f(OCV, SoC)_{(t-1)} - U_{T(t)}}{I_{(t)}}, \tag{2}$$

where R_0 is the internal resistance of the battery cell, $f(OCV, SoC)_{(t-1)}$ is the value of the OCV at the time $(t-1)$, $U_{T(t)}$ is the value of the terminal voltage at the time (t), and $I_{(t)}$ is the instantaneous current at the time (t). Since the internal resistance is based on instantaneous data, it captures the interaction at different temperatures and operating currents. The temperature-effective battery model is completed with the cir-

cuit equations given in equations (3)–(5):

$$\frac{dU_1}{dt} = -\frac{U_1}{R_1C_1} + \frac{1}{C_1}I, \tag{3}$$

$$\frac{dU_2}{dt} = -\frac{U_2}{R_2C_2} + \frac{1}{C_2}I, \tag{4}$$

$$U_T = f(OCV, SoC) - U_1 - U_2 - IR_0. \tag{5}$$

2.2. Parameter identification

The experimental test bench given in Fig. 2 was set up to conduct the experimental studies. The structure includes a DC power supply, DC electronic load, data acquisition system, thermal chamber, and LTO battery cell. The nominal voltage of the LTO battery cell is 2.3 V and its capacity is 40 Ah.

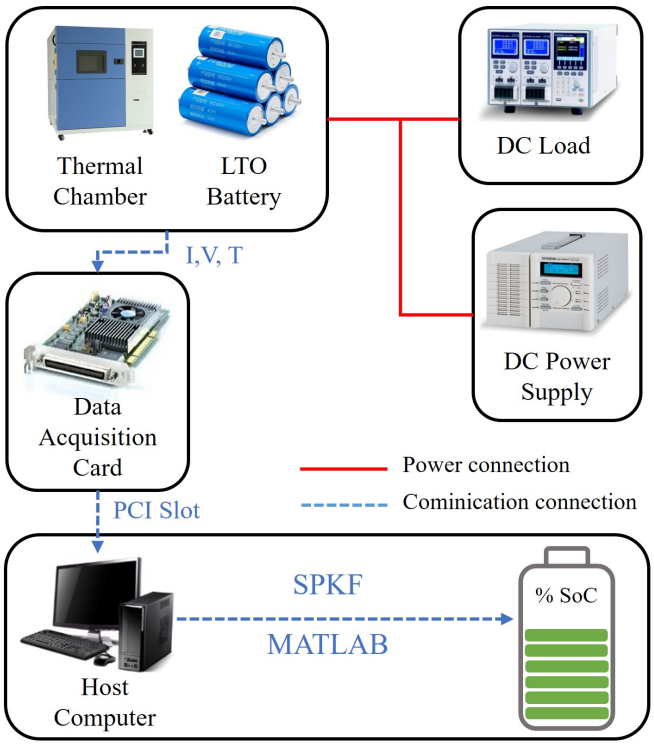

Fig. 2. Diagram of experimental test bench

The relationship between OCV and SoC is obtained experimentally. A gradual discharge process is applied from the fully charged state of the battery until it is completely discharged. During gradual discharge, the battery rests for a sufficient period. Values after rest give the open circuit voltage of the battery. Open circuit voltage analysis of the LTO battery at different temperatures was performed. For the gradual discharge process, 40 A, 8 A, 32 A, 16 A, and 24 A current cycles were applied to the LTO battery under different temperatures, respectively. Figure 3 shows the terminal voltages of the LTO battery under different temperatures after gradual discharge.

In most of the studies conducted with the thermal model, OCV was obtained depending on temperature. However, as seen in Fig. 3, OCV is not affected by different temperatures and different operating currents. Therefore, it is unnecessary to correlate

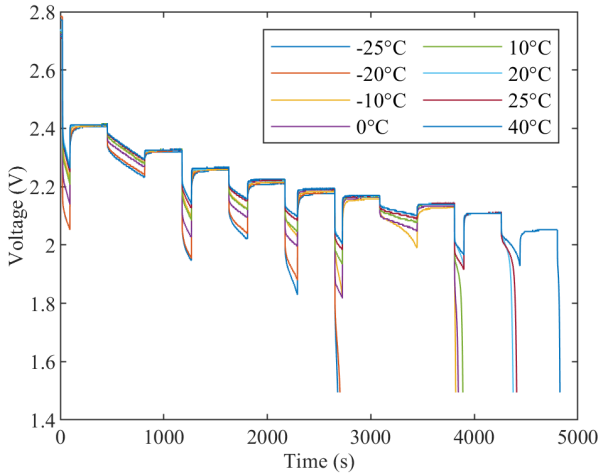

Fig. 3. Gradual discharge of LTO battery under different temperatures

OCV with temperature. The OCV-SoC relationship of the LTO battery was determined by the curve fitting method, as shown in Fig. 4. The polynomial obtained from the curve fitting method is given in equation (6):

$$f(OCV, SoC) = 18.1 \cdot SoC^5 - 43.6 \cdot SoC^4 + 39.8 \cdot SoC^3 - 16.8 \cdot SoC^2 + 3.5 \cdot SoC^1 + 1.8. \tag{6}$$

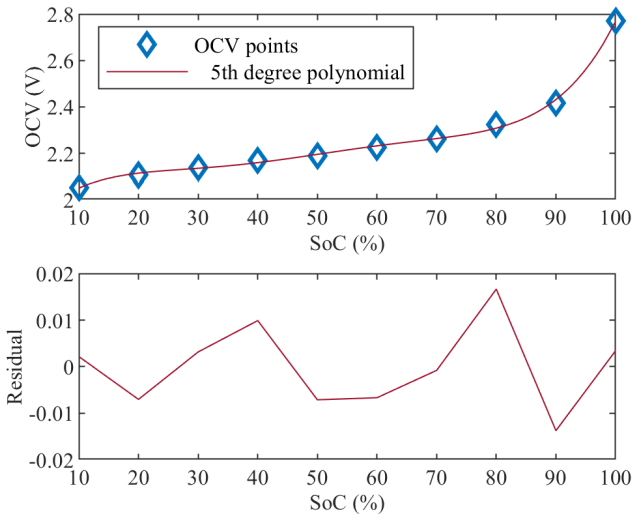

Fig. 4. Graph of the curve fitting

Internal resistance analysis of the LTO battery was performed at different temperatures. The internal resistance graph obtained because of the analysis is shown in Fig. 5. When the results were examined, it was seen that the internal resistance of the LTO battery varied depending on both temperature and SoC.

In studies conducted in the literature, internal resistance has been determined as a polynomial depending on temperature and SoC. However, the resulting polynomial is fixed, not adaptive. Additionally, model complexity increases. Therefore, in this study, internal resistance was determined to adapt to changing conditions without the need for a polynomial. Internal re-

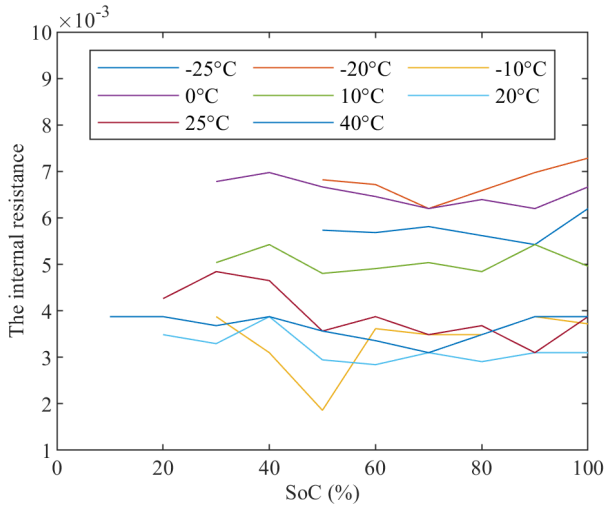

Fig. 5. Internal resistance analysis of the LTO battery under different temperatures

sistance is defined as the ratio of voltage difference to current. Based on its definition, the internal resistance of the LTO battery was determined online as given in equation (2).

RC blocks, which are the other parameters of the equivalent circuit, were determined by the trust-region-reflective-based nonlinear least square method. Internal resistance values are given in Fig. 6, other parameter values are given in Table 1.

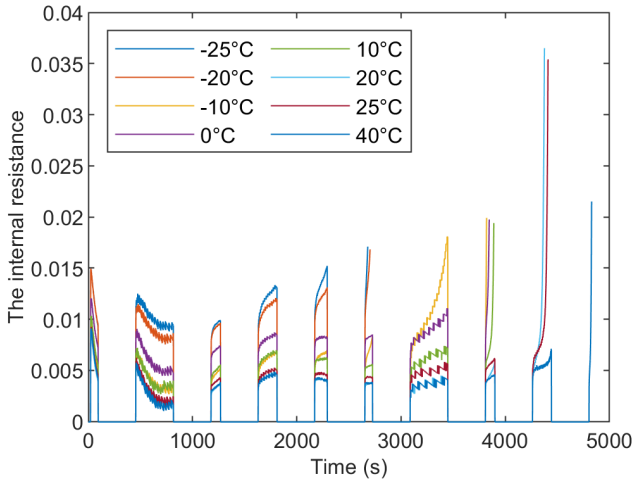

Fig. 6. Internal resistance results of the LTO battery under different temperatures

Table 1
Determined equivalent circuit parameters

LTO cell capacity, C_b:	40 Ah
Polarization resistor, R_1:	0.00026 Ω
Polarization resistor, R_2:	0.000019 Ω
Polarization capacitor, C_1:	1200 F
Polarization capacitor, C_2:	11 000000 F

2.3. Sigma-point Kalman filter

Kalman filters are known as very robust state estimators. EKF and SPKF are improved versions of the conventional Kalman filter [26, 27]. Using Taylor series expansion in EKF, Jacobian matrices are calculated, and the nonlinear model is linearized. This linearization process causes high computational costs and approximation problems. SPKF uses an unscented transformation with a set of sigma points to estimate SoC without linearization. The SPKF addresses high computational costs and approximation problems that arise from the linearization process of the EKF. Therefore, in this study, the SoC of the LTO battery was estimated by the SPKF algorithm. For state estimation in nonlinear systems, the SPKF provides accurate and robust results. The SPKF addresses approximation problems that arise from the linearization process of the extended Kalman filter (EKF). Therefore, in this study, the SoC of the LTO battery was estimated by the SPKF algorithm.

The state-space equation is given by:

$$x_{k+1} = Ax_k + Bu_k\,, \tag{7}$$

$$y_k = Cx_k + Du_k\,, \tag{8}$$

which can be expanded as

$$\begin{bmatrix} SoC_{k+1} \\ U_{1,k+1} \\ U_{2,k+1} \end{bmatrix} = \begin{bmatrix} 1 & 0 & 0 \\ 0 & e^{-\Delta t/C_1R_1} & 0 \\ 0 & 0 & e^{-\Delta t/C_2R_2} \end{bmatrix} \begin{bmatrix} SoC_k \\ U_{1,k} \\ U_{2,k} \end{bmatrix} + \begin{bmatrix} -\Delta t/C_b \\ R_1\left(1-e^{-\Delta t/C_1R_1}\right) \\ R_2\left(1-e^{-\Delta t/C_2R_2}\right) \end{bmatrix} I_k\,, \tag{9}$$

$$V_T = \begin{bmatrix} \dfrac{f\left(OCV_k, SoC_k\right)}{SoC_k} & -1 & -1 \end{bmatrix} \begin{bmatrix} SoC_k \\ U_{1,k} \\ U_{2,k} \end{bmatrix} + R_0 I_k\,, \tag{10}$$

where A, B, C, and D are the coefficient matrices and Δt is the sampling time. SPKF algorithm process is shown in Table 2.

Table 2
Algorithm process of SPKF

Initialization

$$\bar{x}_0^s = E\left[x_0^s\right]$$

$$P_0^s = E\left[\left(x_0^s - \bar{x}_0^s\right)\left(x_0^s - \bar{x}_0^s\right)^T\right]$$

Calculate sigma-points

$$\lambda = \alpha^2(N+\kappa) - N$$

$$X_{k,n-1}^s = \begin{cases} \bar{x}_{n-1}^s & k = 0, \\ \bar{x}_{n-1}^s + \sqrt{(N+\lambda)P_{n-1}^s} & k = 1,\ldots,N, \\ \bar{x}_{n-1}^s - \sqrt{(N+\lambda)P_{n-1}^s} & k = N+1,\ldots,2N, \end{cases}$$

Time update

$$X^x_{k,n-1} = f\left(X^x_{n-1}, X^v_{n-1}, u_{n-1}\right)$$

$$Y_{n|n-1} = h\left(X^x_{n|n-1}, X^w_{n-1}, u_n\right)$$

$$\hat{x}_{n|n-1} = \sum_{k=0}^{2N}\left(w_m^{(k)} X^x_{k,n|n-1}\right)$$

$$P_{n|n-1} = \sum_{k=0}^{2N} w_c^{(k)}\left(X^x_{k,n|n-1} - \hat{x}_{n-1}\right)\left(X^x_{k,n|n-1} - \hat{x}_{n-1}\right)^T$$

Measurement update

$$\overrightarrow{y}_{n-1} = \Sigma_{k=0}^{2N}\left(w_m^{(k)} Y_{k,n|n-1}\right)$$

$$P_{yn} = \sum_{k=0}^{2N} w_c^{(k)}\left(Y_{k,n|n-1} - \overrightarrow{y}_{n-1}\right)\left(Y_{k,n|n-1} - \overrightarrow{y}_{n-1}\right)^T$$

$$P_{xn,yn} = \sum_{k=0}^{2N} w_c^{(k)}\left(X^x_{k,n|n-1} - \hat{x}_{n-1}\right)\left(Y_{k,n|n-1} - \overrightarrow{y}_{n-1}\right)^T$$

$$K_n = P_{xn,yn} P_{yn}^{-1}$$

$$\hat{x}_{n|n} = \hat{x}_{n|n-1} + K_n\left(y_n - \overrightarrow{y}_n\right)$$

$$P_{n|n} = P_{n|n-1} - K_n P_{yn} K_n^T$$

3. RESULTS AND DISCUSSION

In this section, the proposed temperature-effective battery model was tested under different temperatures. Room temperature was chosen as the modeling reference and all parameters were determined at this temperature. The SoC estimation was also made at the same temperature and tested at other temperatures.

3.1. Validation of the temperature-effective battery model

The graphs of voltage comparisons made under different temperatures and their absolute errors are given in Figs. 7–14. When the comparison graphs are examined, it is seen that the errors are almost the same in the no-load condition. At no load, the terminal voltage is equal to the open circuit voltage, and this error is caused by the curve fitting method.

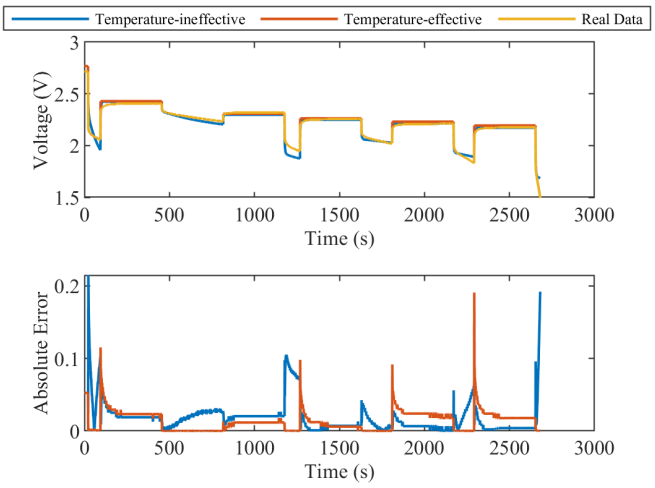

Fig. 7. Model validation at −25°C

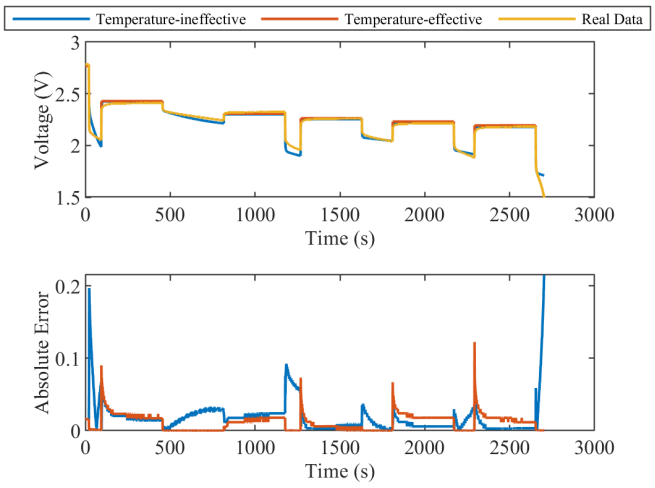

Fig. 8. Model validation at −20°C

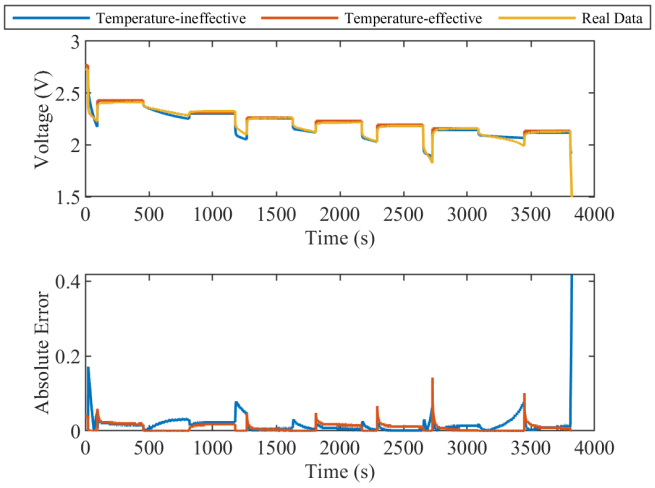

Fig. 9. Model validation at −10°C

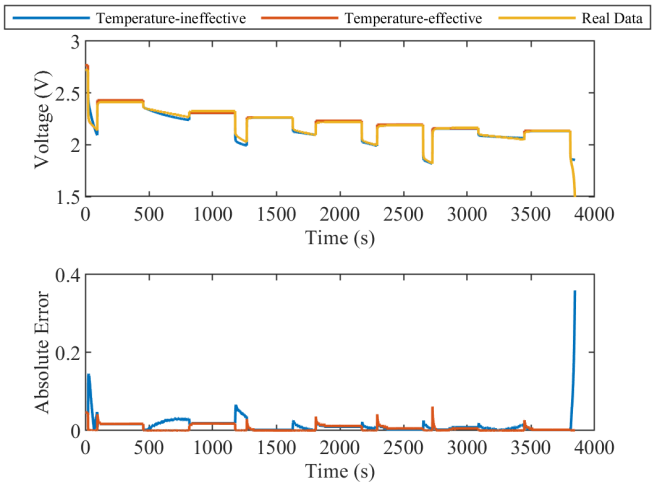

Fig. 10. Model validation at 0°C

When the points under load are examined, it is seen that the temperature-effective model errors are almost zero.

Root mean squared percentage error (RMSPE), mean squared percentage error (MSPE), and mean absolute percentage error (MAPE) metric errors were calculated to better understand the comparison results.

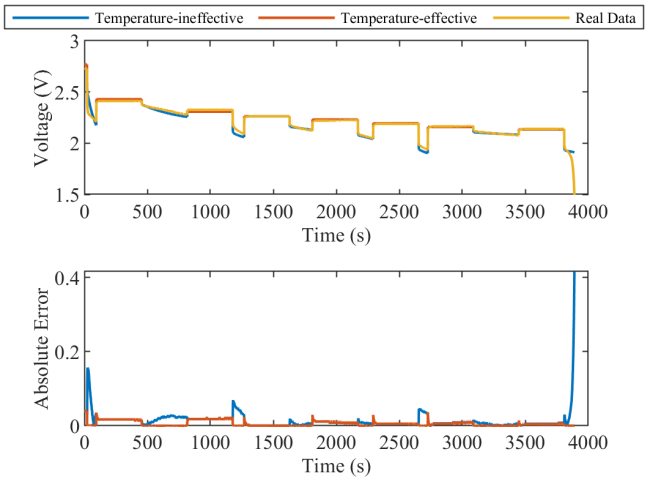

Fig. 11. Model validation at 10°C

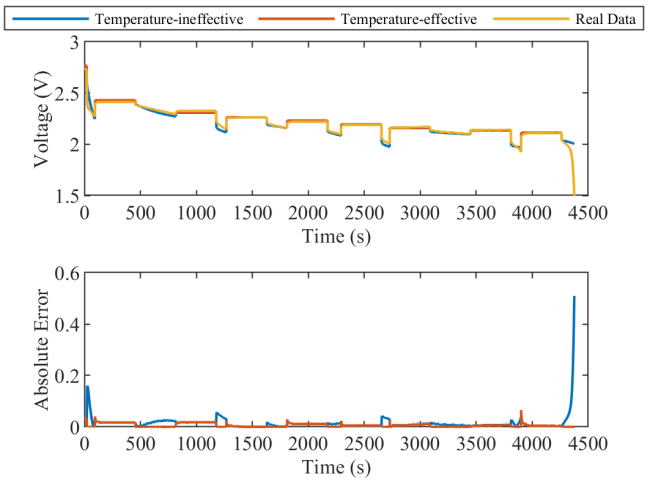

Fig. 12. Model validation at 20°C

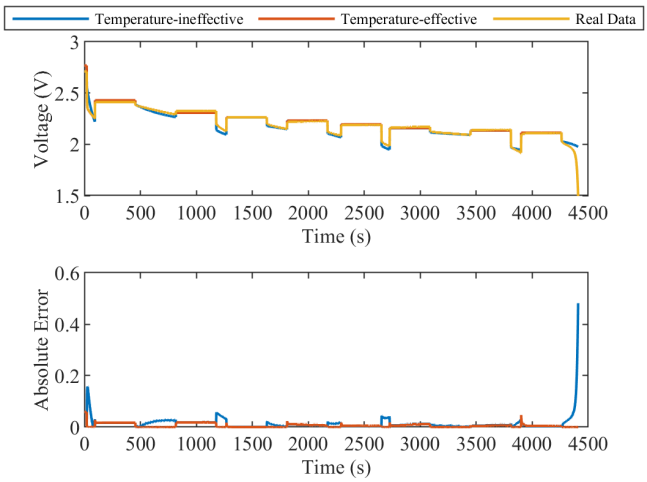

Fig. 13. Model validation at 25°C

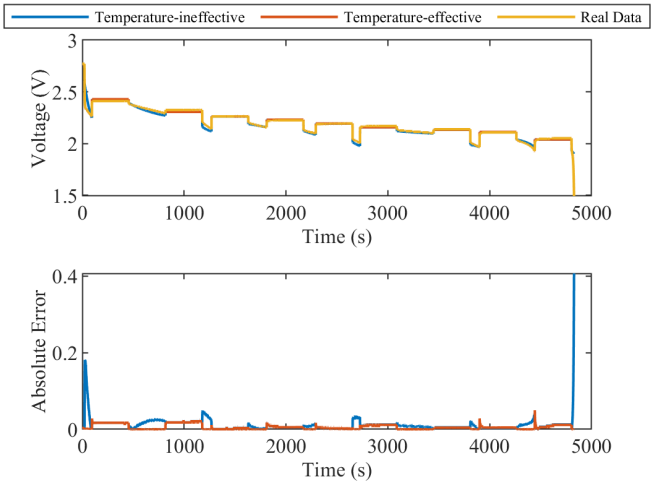

Fig. 14. Model validation at 40°C

Metric error calculations of the model results are given in Table 3.

Table 3
Metric errors of model results

Metric errors	RMSPE		MSPE		MAPE	
Model	TiE	TE	TiE	TE	TiE	TE
−25°C	0.1420	0.0855	0.0202	0.0073	0.8593	0.5988
−20°C	0.1446	0.0701	0.0209	0.0049	0.8302	0.5001
−10°C	0.1333	0.0590	0.0178	0.0035	0.7293	0.3974
0°C	0.1248	0.0431	0.0156	0.0019	0.5889	0.2754
10°C	0.1325	0.0399	0.0175	0.0016	0.5979	0.2635
20°C	0.1636	0.0408	0.0268	0.0017	0.6545	0.2790
25°C	0.1493	0.0405	0.0223	0.0016	0.6366	0.2646
40°C	0.1041	0.0375	0.0108	0.0014	0.5247	0.2533
Improvement range	40–75%		64–94%		30–58%	

When all errors were taken into consideration, the resulting metric errors were examined. It was observed that the temperature-effective (TE) model improved the temperature-ineffective (TiE) model by a minimum of 30% and a maximum of 94%.

3.2. SPKF-based SoC estimation

Room temperature was again chosen as the reference for SoC estimation. SPKF settings were determined based on the best result for this temperature. The state variable was set to $x = \begin{bmatrix}1 & 0 & 0\end{bmatrix}$, and the covariance matrix was set to $P = \text{diag}\begin{bmatrix}10^{-3} & 10^{-3} & 10^{-3}\end{bmatrix}$. The setting of weight matrices are critical parameters that affect SPKF performance. These parameters were adjusted once to examine the temperature effect. Different weight matrices were not set for different temperatures. At room temperature, the weight matrices were set as $Q = \text{diag}\begin{bmatrix}10^{-6} & 10^{-6} & 10^{-6}\end{bmatrix}$, $R = 1$. Fig-

ures 15–22 show test results under different temperatures for SoC estimation.

When the test results were examined, it was seen that the estimation errors with the temperature-ineffective model were up to 10%. On the other hand, the estimation results with the temperature-effective model do not exceed 2%.

Metric errors of SoC comparisons were calculated and are given in Table 4. It is clear from the metric error results that the

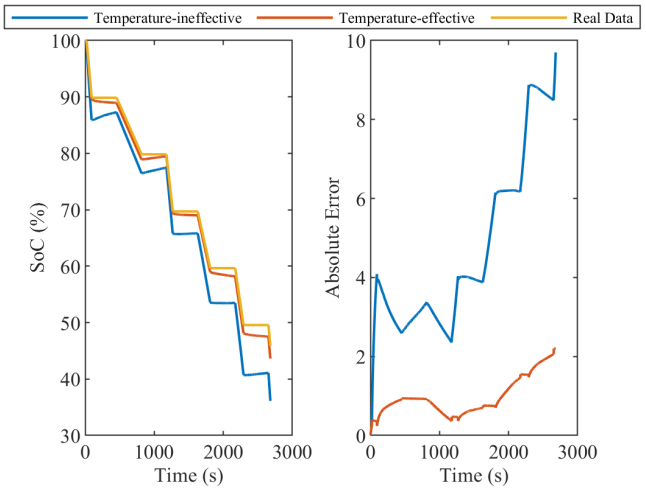

Fig. 15. Validation of the SoC estimation at −25°C

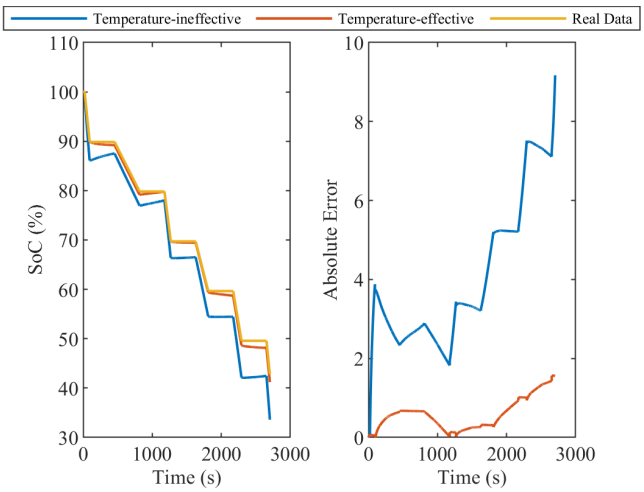

Fig. 16. Validation of the SoC estimation at −20°C

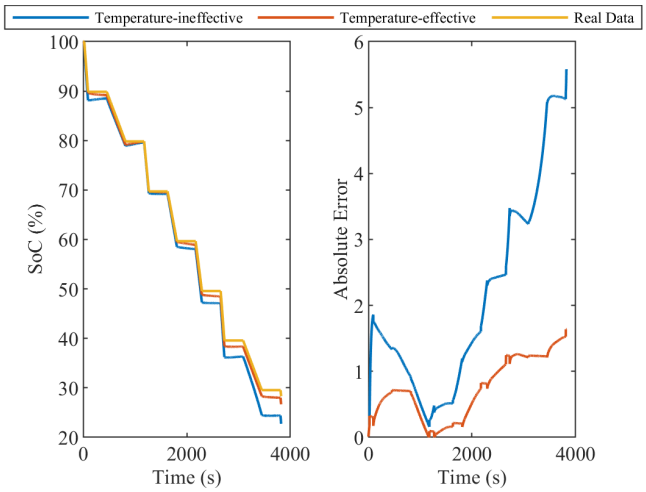

Fig. 17. Validation of the SoC estimation at −10°C

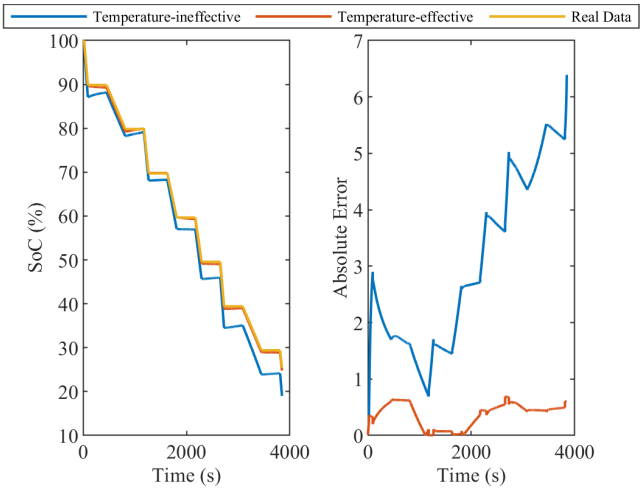

Fig. 18. Validation of the SoC estimation at 0°C

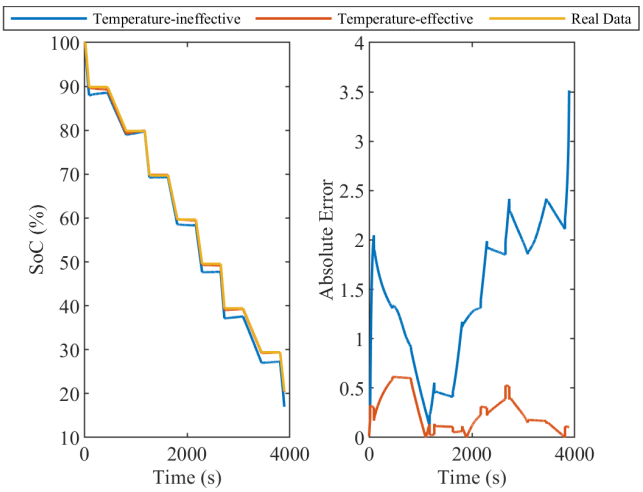

Fig. 19. Validation of the SoC estimation at 10°C

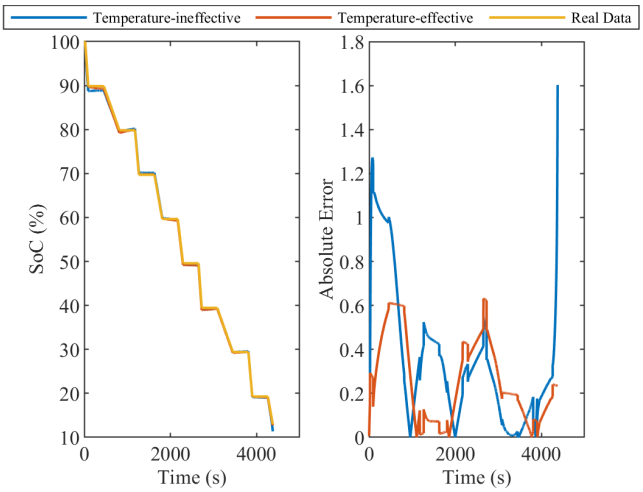

Fig. 20. Validation of the SoC estimation at 20°C

temperature-effective model makes a strong improvement in the SoC prediction results.

Table 4
Metric errors of model results

Metric errors	RMSPE		MSPE		MAPE	
Model	TiE	TE	TiE	TE	TiE	TE
−25°C	0.9126	0.1884	0.8329	0.0355	7.5354	1.5317
−20°C	0.7887	0.1265	0.6221	0.0160	6.5113	0.9434
−10°C	0.7390	0.2295	0.5462	0.0527	5.0497	1.6877
0°C	0.9015	0.0942	0.8128	0.0089	6.8684	0.7613
10°C	0.4180	0.0506	0.1747	0.0026	3.2367	0.4303
20°C	0.1042	0.0633	0.0109	0.0040	0.6675	0.5181
25°C	0.2874	0.0458	0.0826	0.0021	1.7691	0.3724
40°C	0.1123	0.1150	0.0126	0.0132	0.8672	0.7854
Improvement range	2–90%		5–99 %		9–89%	

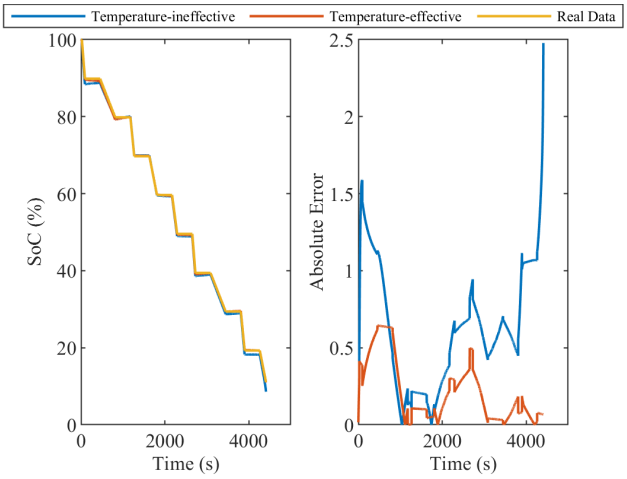

Fig. 21. Validation of the SoC estimation at 25°C

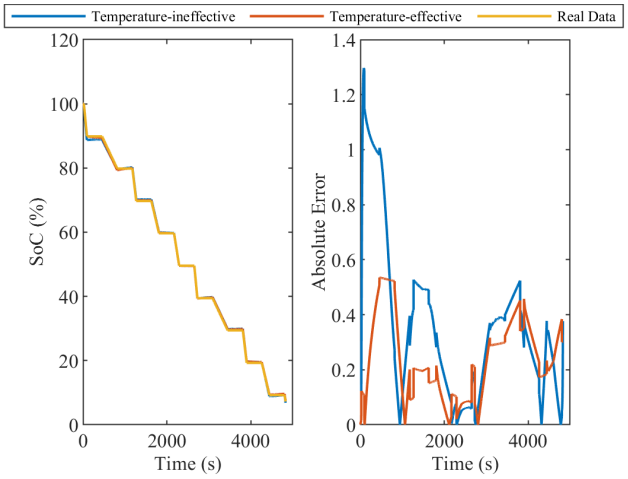

Fig. 22. Validation of the SoC estimation at 40°C

4. CONCLUSIONS

This study develops a new temperature-effective model for LTO batteries. Unlike other studies, the developed model does not require a separate model for temperature. The model incorporates this effect with internal resistance adaptive to terminal voltage, which is directly affected by temperature. The performance of the proposed model and its impact on SoC estimation was evaluated through experimental tests under different operating conditions. The main results are as follows:

1. The internal resistance converges to its value at different temperatures and improves the accuracy of the model.
2. The average root mean square error (RMSE) of the model is within 0.05%, the mean square error (MSE) is within 0.003%, and the mean absolute error (MAE) is within 0.354%.
3. The model improves SoC estimation performance at different temperatures.
4. The SoC estimation converges to an average of 0.11%, 0.02%, and 0.8% in the RMSE, MSE, and MAE metric errors, respectively.

The proposed temperature-effect model is stable and accurate. Compared to previous studies, it offers a simpler solution to different operating conditions. Since it improves SoC estimation, it benefits the design of the battery management system and can be applied in practical applications.

ACKNOWLEDGEMENTS

The authors would like to thank Mersin University BAP Coordination Department (2023-2-TP3-4943) for their financial support.

REFERENCES

[1] J. Zhu *et al.*, "An improved electro-thermal battery model complemented by current dependent parameters for vehicular low temperature application," *Appl. Energy*, vol. 248, pp. 149–161, Aug. 2019, doi: 10.1016/j.apenergy.2019.04.066.

[2] J. Jayaprabakar, J.A. Kumar, J. Parthipan, A. Karthikeyan, M. Anish, and N. Joy, "Review on hybrid electro chemical energy storage techniques for electrical vehicles: Technical insights on design, performance, energy management, operating issues & challenges," *J. Energy Storage*, vol. 72, p. 108689, Nov. 2023, doi: 10.1016/j.est.2023.108689.

[3] A.F. Challoob, N.A. Bin Rahmat, V.K.A.L Ramachandaramurthy, and A.J. Humaidi, "Energy and battery management systems for electrical vehicles: A comprehensive review & recommendations," *Energy Explor. Exploit.*, Jan. 2023, doi: 10.1177/01445987231211943.

[4] G. Yüksek and A. Alkaya, "An Adaptive Energy Management Approach for Battery-Supercapacitor Hybrid Energy Storage System," *Bull. Pol. Acad. Sci. Tech. Sci.*, vol. 72, pp. e150203, doi: 10.24425/bpasts.2024.150203.

[5] G. Yüksek and A. Alkaya, "A novel state of health estimation approach based on polynomial model for lithium-ion batteries," *Int. J. Electrochem. Sci.*, vol. 18, no. 5, p. 100111, 2023, doi: 10.1016/j.ijoes.2023.100111.

[6] Z.N. Ezhyeh, M. Khodaei, and F. Torabi, "Review on doping strategy in Li4Ti5O12 as an anode material for Lithium-ion bat-

teries," *Ceram. Int.*, vol. 49, no. 5. pp. 7105–7141, Mar. 2023, doi: 10.1016/j.ceramint.2022.04.340.

[7] R. Ranjith Kumar, C. Bharatiraja, K. Udhayakumar, S. Devakirubakaran, K.S. Sekar, and L. Mihet-Popa, "Advances in Batteries, Battery Modeling, Battery Management System, Battery Thermal Management, SOC, SOH, and Charge/Discharge Characteristics in EV Applications," *IEEE Access*, vol. 11, pp. 105761–105809, 2023, doi: 10.1109/ACCESS.2023.3318121.

[8] K. Saqli, H. Bouchareb, N.K. M'sirdi, and M. Oudghiri Bentaie, "Lithium-ion battery electro-thermal modelling and internal states co-estimation for electric vehicles," *J. Energy Storage*, vol. 63, p. 107072, Jul. 2023, doi: 10.1016/j.est.2023.107072.

[9] J. Meng, G. Luo, M. Ricco, M. Swierczynski, D.I. Stroe, and R. Teodorescu, "Overview of Lithium-Ion battery modeling methods for state-of-charge estimation in electrical vehicles," *Appl. Sci.*, vol. 8, no. 5, p. 659, Apr. 2018, doi: 10.3390/app8050659.

[10] A.A. Hussein, "An Empirical Capacity Estimation Model for Lithium-ion Battery Cells Using Surface Temperature and Terminal Voltage Measurements," *2023 IEEE Applied Power Electronics Conference and Exposition (APEC)*, Orlando, USA, 2023, pp. 110–113, doi: 10.1109/APEC43580.2023.10131419.

[11] L. Xu, J. Cooper, A. Allam, and S. Onori, "Comparative Analysis of Numerical Methods for Lithium-Ion Battery Electrochemical Modeling," *J. Electrochem. Soc.*, vol. 170, no. 12, p. 120525, Dec. 2023, doi: 10.1149/1945-7111/ad1293.

[12] G. Tucker, R. Drummond, and S.R. Duncan, "Optimal Fast Charging of Lithium Ion Batteries: Between Model-Based and Data-Driven Methods," *J. Electrochem. Soc.*, vol. 170, no. 12, p. 120508, Dec. 2023, doi: 10.1149/1945-7111/ad0ccd.

[13] S. Nejad, D.T. Gladwin, and D.A. Stone, "A systematic review of lumped-parameter equivalent circuit models for real-time estimation of lithium-ion battery states," *J. Power Sources*, vol. 316, pp. 183–196, Jun. 2016, doi: 10.1016/j.jpowsour.2016.03.042.

[14] S. Mao *et al.*, "An Electrical–Thermal Coupling Model with Artificial Intelligence for State of Charge and Residual Available Energy Co-Estimation of LiFePO4 Battery System under Various Temperatures," *Batteries*, vol. 8, no. 10, p. 140, Oct. 2022, doi: 10.3390/batteries8100140.

[15] G. Vennam, A. Sahoo, and S. Ahmed, "A Novel Coupled Electro-thermal-aging Model for Simultaneous SOC, SOH, and Parameter Estimation of Lithium-ion Batteries," *2022 American Control Conference (ACC)*, Atlanta, USA, 2022, pp. 5259–5264, doi: 10.23919/ACC53348.2022.9867320.

[16] H. Bouchareb, K. Saqli, N.K. M'Sirdi and M. Oudghiri, "Observer Design for SOC Estimation of Li-ion Batteries Based on Electro-Thermal Coupled Model," *2021 9th International Renewable and Sustainable Energy Conference (IRSEC)*, Morocco, 2021, pp. 1–6, doi: 10.1109/IRSEC53969.2021.9741140.

[17] A.K. De Souza, G. Plett, and M.S. Trimboli, "Lithium-Ion Battery Charging Control Using a Coupled Electro-Thermal Model and Model Predictive Control," *IEEE Applied Power Electronics Conference and Exposition (APEC)*, New Orleans, USA, 2020, pp. 3534–3539, doi: 10.1109/APEC39645.2020.9124431.

[18] S. Liu, H. Sun, H. Yu, J. Miao, C. Zheng, and X. Zhang, "A framework for battery temperature estimation based on fractional electro-thermal coupling model," *J. Energy Storage*, vol. 63, p. 107042, Jul. 2023, doi: 10.1016/j.est.2023.107042.

[19] C.S. Chin, Z. Gao, and C.Z. Zhang, "Comprehensive electro-thermal model of 26650 lithium battery for discharge cycle under parametric and temperature variations," *J. Energy Storage*, vol. 28, p. 101222, Apr. 2020, doi: 10.1016/j.est.2020.101222.

[20] K. Li, F. Zhou, X. Chen, W. Yang, J. Shen, and Z. Song, "State-of-charge estimation combination algorithm for lithium-ion batteries with Frobenius-norm-based QR decomposition modified adaptive cubature Kalman filter and H-infinity filter based on electro-thermal model," *Energy*, vol. 263, p. 125763, Jan. 2023, doi: 10.1016/J.ENERGY.2022.125763.

[21] A.M.S.M.H.S. Attanayaka, J.P. Karunadasa, and K.T.M.U. Hemapala, "Comprehensive electro-thermal battery-model for Li-ion batteries in microgrid applications," *Energy Storage*, vol. 3, no. 3, p. e230, Jun. 2021, doi: 10.1002/EST2.230.

[22] P. Qin, Y. Che, H. Li, Y. Cai, and M. Jiang, "Joint SOC–SOP estimation method for lithium-ion batteries based on electro-thermal model and multi-parameter constraints," *J. Power Electron.*, vol. 22, no. 3, pp. 490–502, Mar. 2022, doi: 10.1007/s43236-021-00376-9.

[23] H. Pang *et al.*, "A novel extended Kalman filter-based battery internal and surface temperature estimation based on an improved electro-thermal model," *J. Energy Storage*, vol. 41, p. 102854, Sept. 2021, doi: 10.1016/j.est.2021.102854.

[24] M.A. Perez Estevez, S. Calligaro, O. Bottesi, C. Caligiuri, and M. Renzi, "An electro-thermal model and its electrical parameters estimation procedure in a lithium-ion battery cell," *Energy*, vol. 234, p. 121296, Nov. 2021, doi: 10.1016/j.energy.2021.121296.

[25] H. Pang, L. Guo, L. Wu, J. Jin, F. Zhang, and K. Liu, "A novel extended Kalman filter-based battery internal and surface temperature estimation based on an improved electro-thermal model," *J. Energy Storage*, vol. 41, p. 102854, Sep. 2021, doi: 10.1016/J.EST.2021.102854.

[26] A.J. Haug, "Bayesian estimation for target tracking: Part II, the Gaussian sigma-point Kalman filters," *WIREs Comp Stat*, vol. 4, no. 5, pp. 489–497, Sep. 2012, doi: 10.1002/wics.1215.

[27] Y. Muratoğlu and A. Alkaya, "Nonlinear estimator-based state of charge estimation for lithium titanate oxide battery in energy storage systems," *Energy Storage*, vol. 6, no. 1, p. e494, Feb. 2024, doi: 10.1002/EST2.494.